# Experimental Observation of Boron Nitride Chains

**Ovidiu Cretu,[*,†] Hannu-Pekka Komsa,[‡] Ossi Lehtinen,[§] Gerardo Algara-Siller,[§] Ute Kaiser,[§] Kazu Suenaga,[†] and Arkady V. Krasheninnikov[‡,∥]**

[†]Nanotube Research Center, National Institute of Advanced Industrial Science and Technology (AIST), Central 5, 1-1-1 Higashi, Tsukuba, Ibaraki 305-8565, Japan, [‡]Department of Applied Physics, Aalto University, P.O. Box 11100, 00076 Aalto, Finland, [§]Group of Electron Microscopy of Materials Science, Central Facility for Electron Microscopy, University of Ulm, 89081 Ulm, Germany, and [∥]National University of Science and Technology MISiS, Leninsky pr. 4, Moscow 119049, Russian Federation

**ABSTRACT** We report the formation and characterization of boron nitride atomic chains. The chains were made from hexagonal boron nitride sheets using the electron beam inside a transmission electron microscope. We find that the stability and lifetime of the chains are significantly improved when they are supported by another boron nitride layer. With the help of first-principles calculations, we prove the heteroatomic structure of the chains and determine their mechanical and electronic properties. Our study completes the analogy between various boron nitride and carbon polymorphs, in accordance with earlier theoretical predictions.

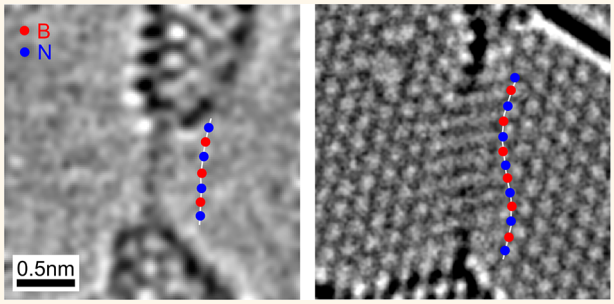


**KEYWORDS:** hexagonal boron nitride · atomic chain · transmission electron microscopy · irradiation · electronic structure calculations

There appears to be a strong correspondence between carbon structures and their boron nitride (BN) counterparts. This was recognized early on by comparing diamond with cubic BN (c-BN) and graphite with hexagonal BN (h-BN). The analogy also extends to molecules, *e.g.*, benzene *vs* borazine, and fullerenes.[1,2] More recently, this has been confirmed by the discovery of carbon and BN nanotubes (NTs),[3−5] as well as by the isolation of single layers of graphene[6] and h-BN.[7,8] The successful *in situ* production and observation of monatomic carbon chains[9] raises the question of whether their BN equivalent exists.

The first theoretical predictions concerning BN chains came before the discovery of graphene.[10] Abdurahman and co-workers established that a linear BN structure was energetically favorable as compared to the zigzag alternatives. They determined that, from the energy point of view, BN chains should be more stable than their carbon counterparts and predicted the existence of both structures. More recently, other theoretical studies have focused on the potential applications of BN chains. The self-assembly of BN chains on graphene was investigated as a possible route to doping,[11] as these formations change the local electronic properties of graphene and provide anchor points for other dopants.

In the present study we report the first *in situ* production and observation of atomic BN chains in an aberration-corrected transmission electron microscope (AC-TEM), by irradiating few-layer h-BN sheets with an electron beam. By using state-of-the-art low-voltage AC-TEM, we are able to observe the formation and subsequent evolution of these structures in real time at subnanometer resolution, while limiting the damage incurred by our specimens. Our experiments show that BN chains can be successfully produced, thus confirming the existing theoretical predictions and furthering the analogy between carbon and BN structures. We find that the chains exist either suspended between two sections of the h-BN lattice or supported by a second h-BN layer, which considerably increases their stability. We provide evidence for the nature of the chains through a combination of high-resolution imaging and theoretical

* Address correspondence to ovidiu.cretu@aist.go.jp.

Received for review August 17, 2014 and accepted October 9, 2014.

**Published online October 09, 2014**
**10.1021/nn5046147**

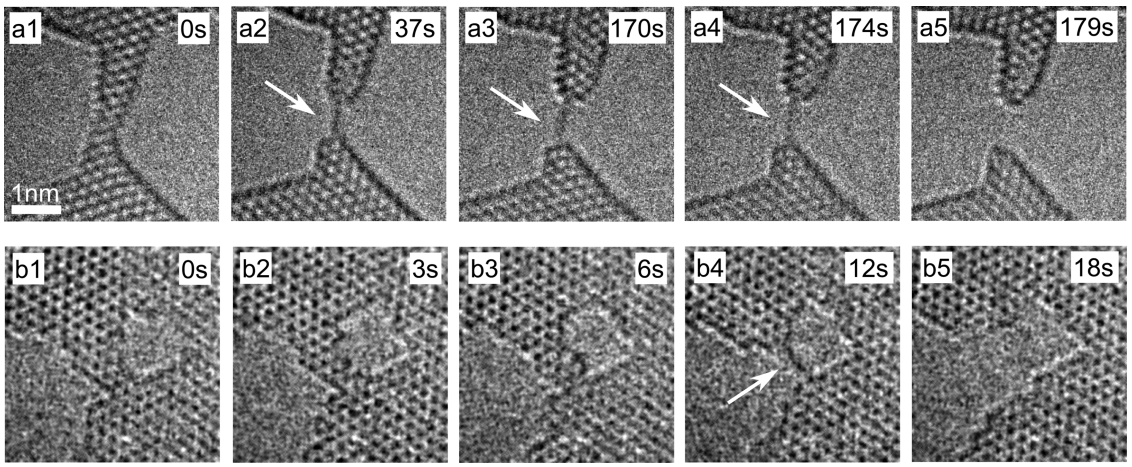


**Figure 1. Two series of images illustrating the formation of suspended atomic chains in bilayer (a) and monolayer (b) h-BN. The data were acquired using 60 kV electrons, with the sample at 650 °C. The images were processed with a median filter and contrast-enhanced for clarity.**

assessment of the energies of the structures. We calculate the mechanical and electronic properties of the chains, study the interaction with the surrounding environment, determine the behavior in the presence of electron irradiation, and compare those to the corresponding characteristics of other candidate and precursor structures. The calculations support our experimental findings and provide additional insights into the physics of these new structures.

## RESULTS

Figure 1 shows image sequences highlighting the formation of suspended atomic chains. The sample was held at 650 °C during the experiments. As a result of electron irradiation, the few-layer h-BN samples became progressively damaged and etched, leading to the formation of large holes. The growth of neighboring holes led to the formation of narrow constrictions in the h-BN lattice. In the case of single-layered samples, these constrictions were narrow nanoribbons (Figure 1b), while for bilayer regions they reconstructed toward tubular structures (Figure 1a), similar to what has earlier been observed in graphene.[12] Most of the times these narrow regions broke and separated the two parts of the lattice. However, prior to breaking, on several occasions, we observed the formation of linear chains. Two examples are shown in Figure 1. The analogous formation of dual chains, under identical conditions, is illustrated in Figure S1. The detailed observation of these structures was limited in all cases by their short lifetime under the electron beam, which was on the order of 1 s.

A single frame extracted from one of the image sequences is shown in Figure 2a; the image has been corrected for nonuniform background, but is otherwise unprocessed. The highlighted area is enlarged in Figure 2b, while a filtered version is shown in Figure 2c. Several dark regions along the direction of the chain can be observed, which are separated by an average distance of 0.25 nm, which is close to the lattice constant of BN.

The short lifetime and low resistance against irradiation of the chains require us to use low exposure times and electron doses. Determining the exact atomic structure of the chain is difficult because of the relatively low signal-to-noise ratio in our images. While our results point toward an alternating B−N configuration, obtaining this information directly would require chains with longer lifetimes or higher stability. Nevertheless, the quality of our data is similar to what has recently been published for very short monatomic carbon chains, which are known to be better suited for electron imaging.[13]

In order to accurately determine the structure and properties of the chains, we performed total energy calculations and molecular dynamics (MD) simulations on several candidate structures. We considered BN, B, and N chains along with the corresponding hexagon-wide nanoribbons, as shown in Figure 3. N chains proved to be unstable under the temperature and pressure conditions used in this study, as expected.[14] Table 1 summarizes the most important results for B and BN structures.

The formation energies were calculated using the following formula: $E^f = E_{tot} - (n_B\mu_B + n_N\mu_N)$, where for BN structures (which are stoichiometric with h-BN) we used $\mu_B + \mu_N = \mu_{h\text{-}BN}$, while for single-element compounds we used the values of the stable phases, $\mu_B = \mu_{\alpha\text{-}B}$ and $\mu_N = (1/2)\mu_{N_2}$. First of all, we predict that isolated one-hexagon-wide nanoribbons are not stable and would transform into two BN chains. This is in agreement with calculations that predict the same effect for single-hexagon carbon nanoribbons,[13,15] due to a balance between bond formation energy and bending energy of the two resulting chains. We also calculated formation energies for larger BN nano-

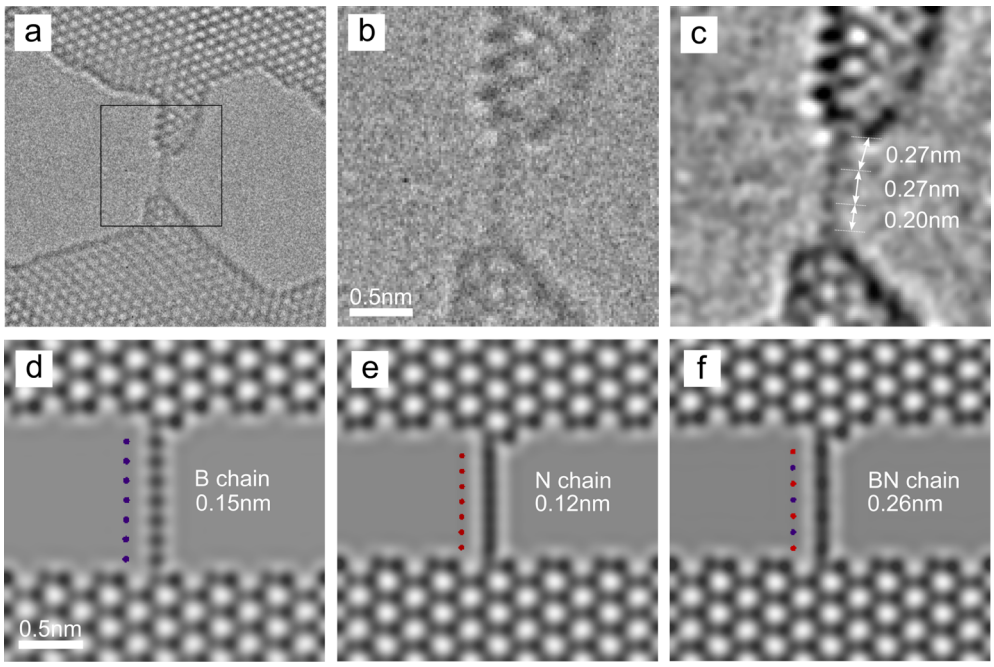


**Figure 2. Atomic structure of the suspended chains. A frame extracted from one of the image series is shown in (a); the image has been corrected for nonuniform background, but is otherwise unprocessed. The data were acquired using 60 kV electrons, at 650 °C. The highlighted area is enlarged in (b). A version of the same area that has been processed with a Gaussian blur filter ($r = 2px$) and contrast-enhanced is shown in (c). Multislice image simulations of B, N, and BN chains are shown in (d)−(f). The effects of sample vibrations and asymmetrical microscope aberrations are omitted in the simulations. B and N atoms are inset in blue and red, respectively.**

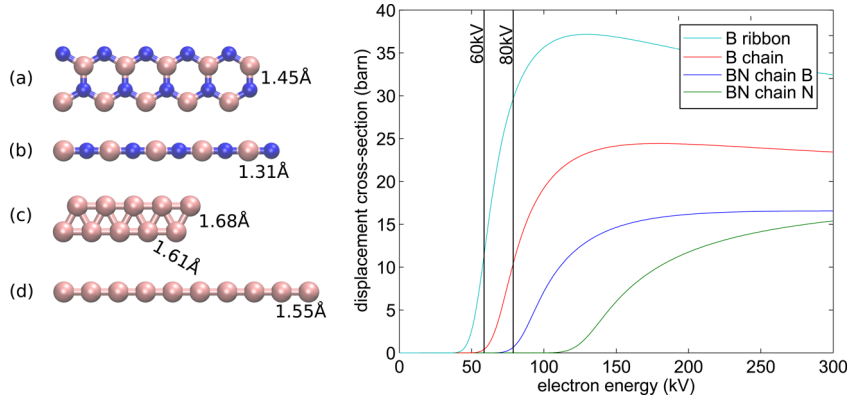


**Figure 3. Atomic structure (left) and electron displacement cross sections (right) of the investigated systems. A narrow BN ribbon and chain are shown in panels (a) and (b), while panels (c) and (d) show hypothetical pure B structures.**

ribbons, finding 5.83 and 5.89 eV for two- and three-hexagon-wide ribbons, respectively. Second, boron is known to form various triangular structures,[16,17] such as the case of the triangular B ribbon considered here, which we also find to be lower in energy than the atomic chains.

Multislice TEM image simulations of the candidates are shown in Figure 2d,e. The periodicities of pure B and N structures are too short (0.15 and 0.12 nm, respectively), whereas the 0.26 nm bond length of BN chain is in good agreement with the experimental observation. The TEM image always shows a projection of the system (on the horizontal plane); this does however set a lower bound on the length, as the projection is always smaller and supports our hypothesis, because B, N (and C) chains would all display much shorter periodicities. Finally, there is a strong possibility that the chain is stretched, which would introduce additional distortion of the bond length; some mechanical deformation is already apparent in the image, because the chain appears curved.

To this end, we carried out molecular dynamics simulations on strained chains. The total run durations in our MD simulations are naturally orders of magnitude smaller than in the experiments, but still serve to provide us with upper bounds. BN (B) chains could be stretched by up to 7% (10%) before breaking, corresponding to bond lengths of 0.14 nm (0.17 nm).

That is, the B structures cannot be strained enough to match the experimental periodicity.

Further analysis of the stability is obtained by calculating the displacement thresholds (and corresponding electron acceleration voltages) required for knock-on displacements, which are shown in Table 1. On the basis of the first value, the temperature-corrected[18] displacement cross sections were calculated, and they are plotted in Figure 3. The data show that BN chains are the most stable under electron irradiation, followed by B chains and B ribbons. The threshold further decreases for wider BN nanoribbons (9/10.5 eV for B/N, respectively, in the case of a two-hexagon ribbon). Thus, all calculations (bond length, formation energy, and displacement threshold) support that the observed structures are BN chains.

We have additionally observed the formation of supported atomic chains, as illustrated in Figure 4. The formation mechanism was similar to the one responsible for the suspended structures: two of the h-BN layers in a trilayer area became damaged and formed one or several narrow constrictions (Figure 4a1), which subsequently reconstructed to chain-like structures (Figure 4a2). The main difference between the suspended and supported cases is the high stability of the supported structures, which determined their long lifetime and allowed for detailed studies. The experiments were performed in a different microscope, where higher electron-accelerating voltages and doses could be used. We have found that the resistance of the supported structures to electron irradiation was higher than that of the supporting h-BN layer. This is illustrated in Figure 4a, which shows a case where two of the h-BN layers are gradually etched, leaving behind several chains which organized into a closed loop. The lifetime of this system was limited only by the etching of the supporting layer, as pictured in the last frame of the sequence.

**TABLE 1. Formation Energy, Displacement Threshold (with the Corresponding Electron Acceleration Voltage), and Maximum Bond Length (with Corresponding Strain) for the Investigated Systems[a]**

| system | $E_f$ (eV) | $T_d$ (eV) [$U$ (kV)] | $b_{max}$ (Å) [$\varepsilon_{max}$ (%)] |
|---|---|---|---|
| BN ribbon | unstable[b] | | |
| BN chain | 1.61 | 17.5/22 [80/125] | 1.4 [7] |
| B ribbon | 0.65 | 11.6 [54] | |
| B chain | 1.69 | 14.7 [68] | 1.7 [10] |

[a] In the BN systems, the first number stands for B, the second for N atoms. [b] Transforms into two BN chains.

The images show regions with high and low contrast. The low-contrast regions appear broadened in a way that would be consistent with rapid movement. Our calculations indicate that BN chains interact very weakly with the substrate layer (see Figure S2 and the associated text). We find binding energies of −0.12 eV/BN unit, which allows for them to undergo rapid movement under the electron beam. Although the interaction with the pristine substrate is minor, the BN chains bind fairly strongly to undercoordinated sites such as vacancies, as arrowed in Figure 4a3 and a5 and confirmed by our calculations. The binding energy of the chains to B vacancies, which are predominantly created under the electron beam, is especially strong and leads to an additional binding energy gain of −2.92 eV per vacancy.

On the other hand, contrary to the case of suspended systems, even one-hexagon-wide supported BN ribbons remain stable because of the interaction between the ribbon edges and the substrate sites (see Figure S3 and associated text). Due to this interaction, which overcomes the van der Waals binding, very thin ribbons in fact prefer to stand up rather than stay parallel to the substrate, thereby gaining up to −0.8 eV/edge site. We can therefore assign the high

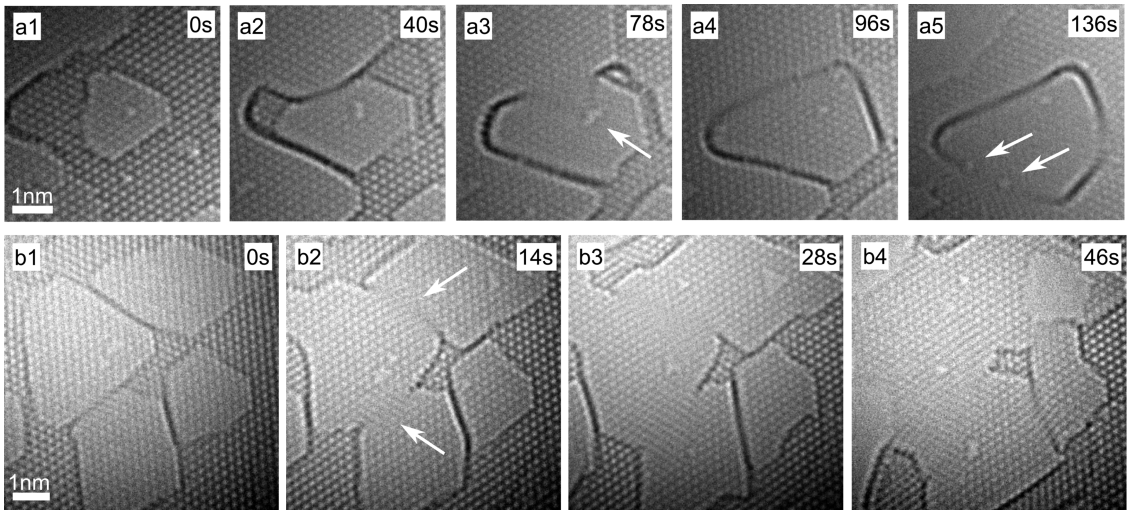


**Figure 4. Image sequences illustrating the formation and evolution of supported atomic chains. The data were acquired using 80 kV electrons, with the sample at 20 °C. The images were contrast-enhanced for clarity.**

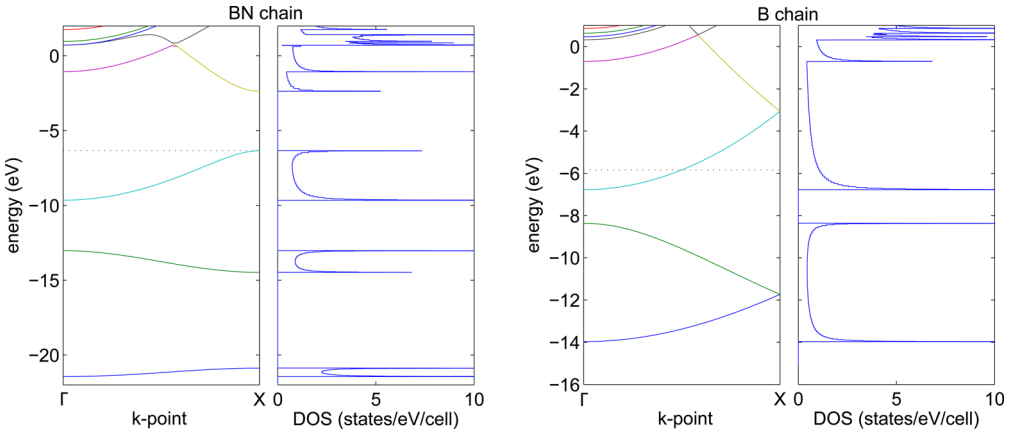


**Figure 5. Band structure and DOS for BN (left) and B (right) chains. Horizontal dotted lines denote the VBM or Fermi level.**

contrast regions to thin BN ribbons standing vertically on the substrate, while the low-contrast areas correspond to vibrating BN chains.

MD simulations also predict that the open ends of chains should be very reactive even with the pristine surface, which is what is also seen experimentally. Figure S4 shows the evolution of a chain that is initially attached to a large defect on the surface (Figure S4a1) and then reattaches to three other locations (a2−a4, arrowed) before finally breaking.

The electronic structure of BN chains is presented in Figure 5. Even though AC-TEM experiments support BN chains, we also calculated the electronic properties for B chains, assuming that they may appear under particular conditions. We find that BN chains are insulating, with a band gap that is close to that of 2D h-BN, while B chains are nearly metallic (undergoing small Peierls distortion accompanied by quadrupling the unit cell size, as the Fermi vector corresponds to quarter filling of the band).

The formation of the chains is governed by atom displacement due to electron irradiation. A detailed discussion of the electron-irradiation damage process in h-BN is given in ref 20. According to ballistic displacement cross-section calculations, the minimum acceleration voltage required for inducing knock-on damage in pristine h-BN is 80 kV. This value decreases to 40 kV in the case of B atoms located at the edges of large holes, while the threshold for N remains above 60 kV in all cases. Under our experimental conditions, we find that vacancies are created and grow below the knock-on threshold. An example is given in Figure S5, which shows single-layer h-BN being progressively damaged under 15 and 30 kV irradiation. Furthermore, it appears that the rate of growth for the large holes increases as the voltage is decreased. This is in agreement with more recent observations on graphene, which show similar effects with 20 kV electrons.[18] This subthreshold damage is likely due to the localized ionization of the specimen because of inelastic interactions with the electron beam, combined with beam-mediated chemical reactions between the sample and residuals in the microscope vacuum (typically $10^{-5}$ Pa).[19] We have investigated a wide range of temperatures and found that the damage rate is only slightly reduced compared to the room-temperature case. An ideal solution would combine subthreshold accelerating voltages (in order to prevent knock-on damage but still allow for sufficient resolution) and ultrahigh vacuum in order to limit the effects of chemical etching.

High-temperature imaging promotes structural reconstructions due to thermal energy, which makes it possible to overcome local potential energy barriers. This comes at the expense of thermal drift, which slightly degrades the image quality. High temperatures also make it possible to evaporate hydrocarbons deposited on the h-BN layers, thus preventing their migration toward the irradiated area during imaging. Our *in situ* experiments were performed far from areas where these impurities agglomerated. Additionally, in all of our cases, the chains formed by the gradual thinning of h-BN nanostructures, and not by the addition of new material/atoms. As such, we are confident that the observed chains are BN-based and not a result of, for example, the migration of carbon atoms in the irradiated area.

According to our calculations, two-hexagon BN nanoribbons are higher in energy than the corresponding chain structures (4.83 eV for three chain units), while three-hexagon nanoribbons are more stable than the corresponding chains (6.44 eV for four chain units). The fact that we have not been able to observe triple chains in our experiments can be explained by the fact that the large energy barrier can only be overcome through interactions with the electrons from the beam, which require several synchronized collisions. The high speed of the incoming electrons (∼0.5c) and the atomic-scale thickness of our samples mean that at any given moment there is only one electron passing through the sample, despite the large beam current densities used, rendering the scenario unlikely.

As B and N atoms are removed from the edges of the nanoribbons, (either through knock-on collisions, in which case B will be displaced first, or *via* chemical etching), they thin down to one-hexagon-wide ribbons, which are unstable and transform into BN chains. It is important to note that this mechanism may exclude the case of pure B structures. Their formation is difficult to understand in a situation where the B atoms are preferential targets for sputtering. The cross sections plotted in Figure 3 show that B ribbons and chains would not be stable under our imaging conditions.

The displacement rate[21] can be calculated as a function of the beam current and displacement cross section. In the case of the supported chains, $p = \sigma j \cong 10^{-3}\ s^{-1}$. This corresponds to lifetimes on the order of several tens of minutes. The lower displacement threshold of the chains (Table 1) compared to that for the h-BN supporting layer[20] explains why the lifetime of these structures is limited by the degradation of the latter, in accordance with what is observed experimentally. This argument however does not hold for the suspended chains, which have much shorter lifetimes despite the lower acceleration voltages used. Strain was also considered as a possible cause of breaking. Calculations predict an ultimate strain upper bound of 7%, which is lower than the 5−12%[22] or the more recently calculated 18−19%[15] for carbon chains. This is introduced due to the degradation of the BN layer on both sides of the chain. Another important cause for mechanical instabilities could be the vibration of the chains. These issues are less important for the supported chains, as the underlying layer gives them the freedom to adapt by changing their anchor points to defects on the surface (Figure 4a3 and a5) or to other points along the edge of the shrinking layer (Figure 4b3). We additionally theorize that changes in the chain structure and bonding could be accommodated by atoms diffusing on the surface of the supporting layer.

It is interesting to compare the chain structures observed in this study with their structural analogues, atomic carbon chains. Using few-layer graphene as a starting material, suspended chains have been obtained and observed inside the TEM by several groups.[13,23−26,28] A common problem is the absence of structural information in the images for the chains themselves, even in cases where the microscope resolution and signal-to-noise ratio should allow for this information to be visible. This is likely due to the vibration of the chains, which introduces blurring in the images and is similar to what we see in the present work. Recent calculations have shown a correlation between the strain in carbon chains and their vibration, which increases with the amount of tension present.[27] Electrically, these chains are very poor conductors when compared to graphene, featuring a band gap that increases with strain.[27,28] This is similar to our calculations, which predict that BN chains are insulating.

Supported carbon chains have also previously been observed.[24,29] They share some common characteristics with our BN structures: they appear to be more stable than the suspended ones, allowing observation times of more than several seconds. They are also mobile on the graphene surface, performing small jumps between intermediate stable positions. Additionally, ref 29 shows the evolution of a chain that has its central part anchored on a point on the surface for several seconds (supplementary movie 2). Although the resolution is not sufficient for unambiguous identification of the structure, one of the possibilities is that it is pinned to a surface defect, in agreement with our observations.

## CONCLUSIONS

To sum up, we have observed the formation and subsequent evolution of atomic boron nitride chains in real time at sub-nanometer resolution, by using low-voltage AC-TEM. We have found that the chains exist either suspended between two parts of the h-BN lattice or supported by a second h-BN layer and found that their stability and lifetime are considerably improved in the latter case. We have presented evidence for the heteroatomic structure of the chains through a combination of high-resolution imaging and energy considerations based on DFT calculations. Our study confirms the existing theoretical predictions and completes the structural analogy between carbon and BN nanomaterials. Our results further indicate that the electron beam is a well-adapted tool for engineering low-dimensional materials with new morphologies and can specifically be used for making atomic chains of ionic materials.

## METHODS

h-BN single crystals were mechanically exfoliated using Scotch tape and transferred to silicon substrates with a layer of thermal oxide. Few-layer flakes were then transferred to TEM grids.[30] Electron irradiation and high-resolution TEM imaging were performed in a modified Jeol JEM-2100F microscope, fitted with a cold field-emission gun and dodecapole-based aberration correctors, operated at 30 and 60 kV[31] and in a FEI Titan 80-300 equipped with a Schottky-type field-emission gun and a postspecimen hexapole aberration corrector, operated at 80 kV. The suspended chains were held at 650 °C by using a heating specimen holder (Jeol EM-21130), in which the temperature of the crucible where the sample grid was located was monitored by a thermocouple. The supported chains were imaged at room temperature throughout the experiments. A beam current density of $\sim 10^6 e/nm^2\ s$ was used for imaging the suspended chains and up to $\sim 10^7 e/nm^2\ s$ for the supported chains. The samples were monitored by acquiring image sequences with an exposure time of ~1 s; the overall frame rate

was lower due to the data transfer overhead. The images were processed using ImageJ.[32] Multislice TEM image simulations were performed using the QSTEM package.[33]

Density-functional theory (DFT) calculations were carried out in the plane-wave basis within the projector-augmented wave scheme as implemented in VASP.[34,35] We adopted the Perdew–Burke–Ernzerhof exchange–correlation functional,[36] and in the case of supported chain calculations the van der Waals interactions were accounted for.[37] Total energies were calculated using a 500 eV cutoff and k-point density of 25 k-points·Å or higher. The energy cutoff was lowered to 400 eV in the DFT molecular dynamics runs. Displacement thresholds were evaluated by running sets of MD calculations, where the initial kinetic energy of the displaced ion was varied in order to find the energy at which the displacement takes place.[38] The cross sections were then estimated on the basis of the McKinley–Feshbach formalism,[39] taking into account the thermal motion of the ions.[18]

*Conflict of Interest:* The authors declare no competing financial interest.

*Acknowledgment.* O.C. and K.S. acknowledge support from a JST Research Acceleration program. A.V.K. and H.-P.K. acknowledge support from the Academy of Finland through projects 266924 and 263416 and further thank CSC Finland for generous grants of computer time. O.L., G.A.-S., and U.K. acknowledge financial support by the DFG and the Ministry of Science, Research and the Arts (MWK) of Baden-Wuerttemberg in the frame of the SALVE (Sub Angstrom Low-Voltage Electron microscopy) project. A.V.K. further thanks the Ministry of Education and Science of the Russian Federation in the framework of Increase Competitiveness Program of NUST "MISiS" (No 3-2014-010). O.L. acknowledges financial support by the Finnish Cultural Foundation.

*Supporting Information Available:* Additional content includes image sequences illustrating the formation of suspended dual chains and evolution of open-ended supported chains, calculations of the interaction between supported BN chains and ribbons and the supporting layer, and image sequences showing damage creation in BN by subthreshold irradiation. This material is available free of charge *via* the Internet at http://pubs.acs.org.

## REFERENCES AND NOTES

1. Kroto, H. W.; Heath, J. R.; O'Brien, S. C.; Curl, R. F.; Smalley, R. E. C60: Buckminsterfullerene. *Nature* **1985**, *318*, 162–163.
2. Golberg, D.; Bando, Y.; Stéphan, O.; Kurashima, K. Octahedral Boron Nitride Fullerenes Formed by Electron Beam Irradiation. *Appl. Phys. Lett.* **1998**, *73*, 2441.
3. Iijima, S. Helical Microtubules of Graphitic Carbon. *Nature* **1991**, *354*, 56–58.
4. Chopra, N. G.; Luyken, R. J.; Cherrey, K.; Crespi, V. H.; Cohen, M. L.; Louie, S. G.; Zettl, A. Boron Nitride Nanotubes. *Science* **1995**, *269*, 966–967.
5. Ayala, P.; Arenal, R.; Loiseau, A.; Rubio, A.; Pichler, T. The Physical and Chemical Properties of Heteronanotubes. *Rev. Mod. Phys.* **2010**, *82*, 1843–1885.
6. Novoselov, K. S.; Geim, A. K.; Morozov, S. V.; Jiang, D.; Zhang, Y.; Dubonos, S. V.; Grigorieva, I. V.; Firsov, A. A. Electric Field Effect in Atomically Thin Carbon Films. *Science* **2004**, *306*, 666–669.
7. Novoselov, K. S.; Jiang, D.; Schedin, F.; Booth, T. J.; Khotkevich, V. V.; Morozov, S. V.; Geim, A. K. Two-Dimensional Atomic Crystals. *Proc. Natl. Acad. Sci. U.S.A.* **2005**, *102*, 10451–10453.
8. Song, L.; Ci, L.; Lu, H.; Sorokin, P. B.; Jin, C.; Ni, J.; Kvashnin, A. G.; Kvashnin, D. G.; Lou, J.; Yakobson, B. I.; *et al.* Large Scale Growth and Characterization of Atomic Hexagonal Boron Nitride Layers. *Nano Lett.* **2010**, *10*, 3209–3215.
9. Troiani, H. E.; Miki-Yoshida, M.; Camacho-Bragado, G. A.; Marques, M. A. L.; Rubio, A.; Ascencio, J. A.; Jose-Yacaman, M. Direct Observation of the Mechanical Properties of Single-Walled Carbon Nanotubes and Their Junctions at the Atomic Level. *Nano Lett.* **2003**, *3*, 751–755.
10. Abdurahman, A.; Shukla, A.; Dolg, M. Ab Initio Many-Body Calculations on Infinite Carbon and Boron-Nitrogen Chains. *Phys. Rev. B* **2002**, *65*, 115106.
11. Ozcelik, V. O.; Ciraci, S. Self-Assembly Mechanisms of Short Atomic Chains on Single-Layer Graphene and Boron Nitride. *Phys. Rev. B* **2012**, *86*, 155421.
12. Algara-Siller, G.; Santana, A.; Onions, R.; Suyetin, M.; Biskupek, J.; Bichoutskaia, E.; Kaiser, U. Electron-Beam Engineering of Single-Walled Carbon Nanotubes from Bilayer Graphene. *Carbon* **2013**, *65*, 80–86.
13. Casillas, G.; Mayoral, A.; Liu, M.; Ponce, A.; Artyukhov, V. I.; Yakobson, B. I.; Jose-Yacaman, M. New Insights Into The Properties and Interactions of Carbon Chains as Revealed by HRTEM and DFT Analysis. *Carbon* **2014**, *66*, 434–441.
14. Buchsbaum, S.; Mills, R. L.; Schiferl, D. Phase Diagram of Nitrogen Determined By Raman Spectroscopy from 15 to 300 K at Pressures to 52 GPa. *J. Phys. Chem.* **1984**, *88*, 2522.
15. Liu, M.; Artyukhov, V. I.; Lee, H.; Xu, F.; Yakobson, B. I. Carbyne from First Principles: Chain of C Atoms, a Nanorod or a Nanorope. *ACS Nano* **2013**, *7*, 10075–10082.
16. Boustani, I. Systematic ab Initio Investigation of Bare Boron Clusters: Determination of the Geometry and Electronic Structures of Bn (n=2–14). *Phys. Rev. B* **1997**, *55*, 16426.
17. Wu, X.; Dai, J.; Zhao, Y.; Zhuo, Z.; Yang, J.; Zeng, X. C. Two-Dimensional Boron Monolayer Sheets. *ACS Nano* **2012**, *6*, 7443–7453.
18. Meyer, J.; Eder, F.; Kurasch, S.; Skakalova, V.; Kotakoski, J.; Park, H. J.; Roth, S.; Chuvilin, A.; Eyhusen, S.; Benner, G.; *et al.* Accurate Measurement of Electron Beam Induced Displacement Cross Sections for Single-Layer Graphene. *Phys. Rev. Lett.* **2012**, *108*, 196102.
19. Egerton, R. F. Mechanisms of Radiation Damage in Beam-Sensitive Specimens, for TEM Accelerating Voltages between 10 and 300 kV. *Microsc. Res. Techniq.* **2012**, *75*, 1550–1556.
20. Kotakoski, J.; Jin, C. H.; Lehtinen, O.; Suenaga, K.; Krasheninnikov, A. V. Electron Knock-On Damage in Hexagonal Boron Nitride Monolayers. *Phys. Rev. B* **2010**, *82*, 113404.
21. Banhart, F. Irradiation Effects in Carbon Nanostructures. *Rep. Prog. Phys.* **1999**, *62*, 1181.
22. Nair, A. K.; Cranford, S. W.; Buehler, M. J. The Minimal Nanowire: Mechanical Properties of Carbyne. *EPL* **2011**, *95*, 16002.
23. Jin, C.; Lan, H.; Peng, L.; Suenaga, K.; Iijima, S. Deriving Carbon Atomic Chains from Graphene. *Phys. Rev. Lett.* **2009**, *102*, 205501.
24. Chuvilin, A.; Meyer, J. C.; Algara-Siller, G.; Kaiser, U. From Graphene Constrictions to Single Carbon Chains. *New J. Phys.* **2009**, *11*, 083019.
25. Song, B.; Schneider, G. F.; Xu, Q.; Pandraud, G.; Dekker, C.; Zandbergen, H. Atomic-Scale Electron-Beam Sculpting of Near-Defect-Free Graphene Nanostructures. *Nano Lett.* **2011**, *11*, 2247–2250.
26. Robertson, A. W.; Warner, J. H. Atomic Resolution Imaging of Graphene by Transmission Electron Microscopy. *Nanoscale* **2013**, *5*, 4079–4093.
27. Artyukhov, V. I.; Liu, M.; Yakobson, B. I. Mechanically Induced Metal–Insulator Transition in Carbyne. *Nano Lett.* **2014**, *14*, 4224–4229.
28. Cretu, O.; Botello-Mendez, A. R.; Janowska, I.; Pham-Huu, C.; Charlier, J.-C.; Banhart, F. Electrical Transport Measured in Atomic Carbon Chains. *Nano Lett.* **2013**, *13*, 3487–3493.
29. Meyer, J. C.; Girit, C. O.; Crommie, M. F.; Zettl, A. Imaging and Dynamics of Light Atoms and Molecules on Graphene. *Nature* **2008**, *454*, 319–322.
30. Pacilé, D.; Meyer, J. C.; Girit, Ç. Ö.; Zettl, A. The Two-Dimensional Phase of Boron Nitride: Few-Atomic-Layer Sheets and Suspended Membranes. *Appl. Phys. Lett.* **2008**, *92*, 133107.
31. Sasaki, T.; Sawada, H.; Hosokawa, F.; Kohno, Y.; Tomita, T.; Kaneyama, T.; Kondo, Y.; Kimoto, K.; Sato, Y.; Suenaga, K. Performance of Low-Voltage STEM/TEM with Delta Corrector and Cold Field Emission Gun. *J. Electron Microsc.* **2010**, *59* (Suppl), S7–S13.

32. Rasband, W. S. *ImageJ*; U.S. National Institutes of Health, Bethesda, MD, USA, http://imagej.nih.gov/ij/, 1997–2014.
33. Koch, C. T. Determination of Core Structure Periodicity and Point Defect Density along Dislocations. Ph.D. thesis, Arizona State University, 2002.
34. Kresse, G.; Hafner, J. Ab Initio Molecular Dynamics for Liquid Metals. *Phys. Rev. B* **1993**, *47*, 558.
35. Kresse, G.; Furthmüller, J. Efficiency of Ab-Initio Total Energy Calculations for Metals and Semiconductors Using a Plane-Wave Basis Set. *Comput. Mater. Sci.* **1996**, *6*, 15–50.
36. Perdew, J. P.; Burke, K.; Ernzerhof, M. Generalized Gradient Approximation Made Simple. *Phys. Rev. Lett.* **1996**, *77*, 3865–3868.
37. Grimme, S. Semiempirical GGA-Type Density Functional Constructed with a Long-Range Dispersion Correction. *J. Comput. Chem.* **2006**, *27*, 1787–1799.
38. Komsa, H.-P.; Kotakoski, J.; Kurasch, S.; Lehtinen, O.; Kaiser, U.; Krasheninnikov, A. V. Two-Dimensional Transition Metal Dichalcogenides under Electron Irradiation: Defect Production and Doping. *Phys. Rev. Lett.* **2012**, *109*, 035503.
39. McKinley, W. A., Jr.; Feshbach, H. The Coulomb Scattering of Relativistic Electrons by Nuclei. *Phys. Rev.* **1948**, *74*, 1759.